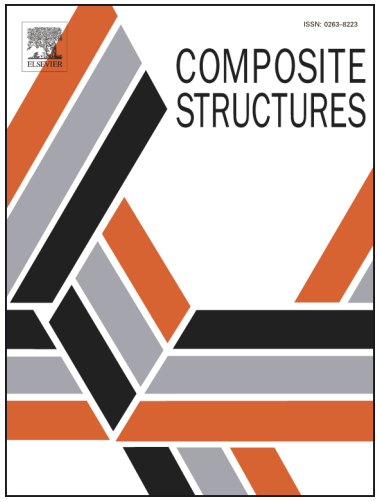

Evaluation of cross-ply laminate stiffness with a non-uniform distribution of transverse matrix cracks by means of a computational meso-mechanic model

Néstor Darío Barulich, Luis Augusto Godoy, Patricia Mónica Dardati

PII: S0263-8223(17)33021-0
DOI: https://doi.org/10.1016/j.compstruct.2017.11.063
Reference: COST 9129

To appear in: *Composite Structures*

Received Date: 15 September 2017
Revised Date: 14 November 2017
Accepted Date: 21 November 2017

Please cite this article as: Barulich, N.D., Godoy, L.A., Dardati, P.M., Evaluation of cross-ply laminate stiffness with a non-uniform distribution of transverse matrix cracks by means of a computational meso-mechanic model, *Composite Structures* (2017), doi: https://doi.org/10.1016/j.compstruct.2017.11.063

Evaluation of cross-ply laminate stiffness with a non-uniform distribution of transverse matrix cracks by means of a computational meso-mechanic model

Néstor Darío Barulich[*1,2], Luis Augusto Godoy[1,3], Patricia Mónica Dardati[2]

1: Instituto de Estudios Avanzados en Ingeniería y Tecnología, IDIT UNC-CONICET, Avda. Vélez Sarsfield 1611, Ciudad Universitaria, X5016GCA – Córdoba, Argentina

2: Facultad Regional Córdoba, Universidad Tecnológica Nacional, Maestro M. López esq. Cruz Roja Argentina, X5016ZAA – Córdoba, Argentina

3: Facultad de Ciencias Exactas, Físicas y Naturales, Universidad Nacional de Córdoba, Avda. Vélez Sarsfield 1611, Ciudad Universitaria, X5016GCA – Córdoba, Argentina

Abstract

This work addresses the evaluation of the stiffness of fiber-reinforced composite laminates, by means of a computational meso-mechanic model, considering two non-uniformly spaced transverse matrix cracks. Laminates with $[0_n/90_8]_S$ and $[90_8/0_n]_S$, with n = 1 and 8, have been studied. The meso-mechanic model includes a three dimensional Finite Element continuum model at meso-scale and the macro-scale contains a classical thin laminated plate model. Periodic boundary conditions were used and the stress resultants were evaluated accounting for the equivalence of mechanical power between scales (Hill-Mandel principle). The results obtained with the present model showed good agreement with numerical and experimental data reported in the literature. A parametric analysis allowed identifying the stiffness components which are more influenced by a non-uniform crack distribution. The results suggest that the model with uniformly distributed cracks underestimates the in-plane and bending stiffness, while the bending-extension coupling stiffness components are overestimated.

Keywords: composite laminate; intra-laminar cracks; finite elements; plate homogenization

1 Introduction

* nbarulich@frc.utn.edu.ar

Polymer-matrix laminated composites are important structural components in engineering structures, for that reason there is an increasing interest in understanding their behavior under different loads during manufacturing and service. One of the first damage modes that takes place in a laminate is the appearance of matrix cracks in lamina spanning the complete ply thickness and running parallel to the fibers; they are also known as ply cracks, intra-laminar cracks, or transverse matrix cracks. Transverse matrix cracks are generated by tensile and shear stresses in a lamina of the laminate following the growth of microscopic defects into meso-scale cracks [1]. Transverse matrix cracks leave the fibers unprotected from chemical gas or liquid agents. These transverse matrix cracks seldom produce a catastrophic failure of the composite component but the reduction in plate stiffness can affect the structure functionality and can also trigger other failure modes as delamination, fiber breakage, and fatigue life reduction ([1] - [3]). Therefore, understanding stiffness reduction in laminates is a critical aspect in structural functionality and failure.

Experimental studies are crucial for discovering underlying failure and deformation mechanisms but they are always costly and time-consuming, making computational models a proper powerful tool to exploit experimental evidence and reduce the number of laboratory tests. Models with various levels of complexity have been reported in the literature for the prediction of laminate stiffness reduction due to transverse matrix cracks, starting from the basic Ply Discount method ([4], [5]), then models based in continuum or discrete damage mechanics ([6], [7]), Crack Opening Displacement (COD) methods ([3]), variational methods ([8] - [10]), synergistic damage mechanics ([16], [17]), and two-scale numerical models ([2], [3], [18] - [21]). Two-scale models have the advantage of presenting a minimum of approximations and having the possibility to account for more details than other approaches.

Models for flexural stiffness reduction due to transverse matrix cracks confront more difficulties than the models for in-plane stiffness reduction. Also, as unsymmetrical laminates present extension-bending coupling, modeling such laminates demands specific formulations. Therefore, just a limited number of works can be found on flexure deformations compared with

those on in-plane deformations (see for example [1], [3], [5], [20], [22]). Earlier works on flexural deformations and transverse cracks such as [11] based on a self-consistent model for lamina properties [12] can be found. In the last two years, the procedure reported by Makins and Adali [11] to obtain the reduced flexure stiffness was used in [13] - [15] for structural analysis. Recently, Hajikazemi et al. [10], while presenting a new variational approach, summarized the contributions available in the literature about modeling flexure stiffness reduction due to transverse matrix cracks, highlighting limitations and concepts involved in each approach covering 19 articles published between 1994 [23] and 2016 [22]; the interested reader can refer to Hajikazemi et al. [10] and works cited therein. Among others, the works by Adumitroaie and Barbero [16] and Hajikazemi et al. ([9], [10]) can address general in-plane and out-of-plane bending deformations in unsymmetrical laminates. Adumitroaie and Barbero [16] have presented a synergistic damage mechanic model merging COD and continuum damage mechanics concepts. Hajikazemi et al. [9] have used a stress-based variational approach for the analysis of general symmetric or unsymmetric cross-ply laminates subjected to out-of-plane bending and biaxial loads; this formulation was extended to account for in-plane shear loads, torsional moments and temperature change [10]. Both formulations in [9] and [10] use the ply-refinement technique obtaining similar results when comparing with numerical models based on Finite Elements or Boundary Elements.

Most single-scale models, as those mentioned above, were developed for practical use demanding a low computer cost which required some simplifications but, at the same time, these simplifications impose restrictions in the range of application of those approximated models. For example, some approaches are restricted to symmetric or balanced laminates and others are limited to in-plane loads as pointed out in [16], among others. A common approximation involves considering uniformly spaced cracks; this provides a reasonable estimate as the crack density grows, but the actual crack distribution is always non-uniform, as experimental studies report ([20], [24]).

A limited number of studies can be found in which the crack distribution is considered non-uniform. Silberschmidt [25] evaluated the changes in stresses redistributions among laminas of cross-ply laminates and Wang *et al.* [26] and Silberschmidt [27] discuss the evolution of transverse cracks with non-uniformly distributed transverse matrix cracks. But, just a few works reported on the stiffness degradation due to non-uniformly located transverse matrix cracks: McCartney and Schoeppner [28] analyzed the in-plane elastic modulus of multi-ply cross-ply symmetric laminates with non-uniformly spaced cracks by means of an approximate analytical model. Loukil *et al.* [29] evaluated the in-plane modulus of cross-ply laminates with transverse cracks in internal and external laminas, called internal and external cracks, by means of a two-dimensional Finite Element model considering a non-uniform crack distribution. Thus, there is a void in the assessment of the complete stiffness matrix in laminates with non-uniform transverse crack distributions.

This work presents the evaluation of the reduced in-plane, bending, and bending-extension coupling stiffness of a fiber-reinforced laminated composite considering a non-uniform distribution of transverse matrix cracks. Only cross-ply laminates are analyzed using a meso-mechanic model. The meso-scale includes a three-dimensional Finite Element continuum solid to model the stress state in the laminate, with the domain comprising the complete laminate thickness and incorporating two transverse matrix cracks, while the macro-scale contains a classical thin laminated plate model.

2 Methodology

The model presented in this work makes use of two scales of analysis: one is the meso-scale, which considers the laminate as a three-dimensional continuum which is discretized using Finite Elements; and the second scale, called macro-scale, uses the classical model for thin laminated plates under small deformations. Each lamina was considered to be made of a linear elastic transversely isotropic material. Similar models were presented in the literature allowing for membrane (in-plane) deformations ([2], [30], [31], [18], [19]) or both membrane and bending deformations ([3], [32], [20], [33] - [35]). The meso-scale and the macro-scale are connected by the

boundary conditions used in the meso-scale and by the equations to obtain the stress resultants of the macro-scale; those connections are presented in detail in the next sections.

The three-dimensional domain of analysis in the meso-scale, called Representative Volume Element (RVE), spans the complete laminate thickness h (Figure 1 and 2a) and contains two transverse matrix cracks in each cracked lamina. In order to study the influence of non-uniformly located cracks, they were distributed as shown in Figure 1. A non-uniformity parameter k, ranging from zero to unity $0 \leq k \leq 1$, was defined as

$$k = \frac{d - t_k / 2}{L - t_k / 2} \tag{1}$$

where t_k is the cracked-ply thickness, d is the distance between cracks, and L is half the length of the RVE in x direction, as shown in Figure 1. All laminates in Figure 1 have a crack density $\lambda = 1/L$.

In order to model crack closure, which occurs under flexure deformations, contact without friction was assumed and it was implemented using a penalty approach available in ABAQUS [36]. The contact between crack surfaces includes only normal compressive stresses between surfaces.

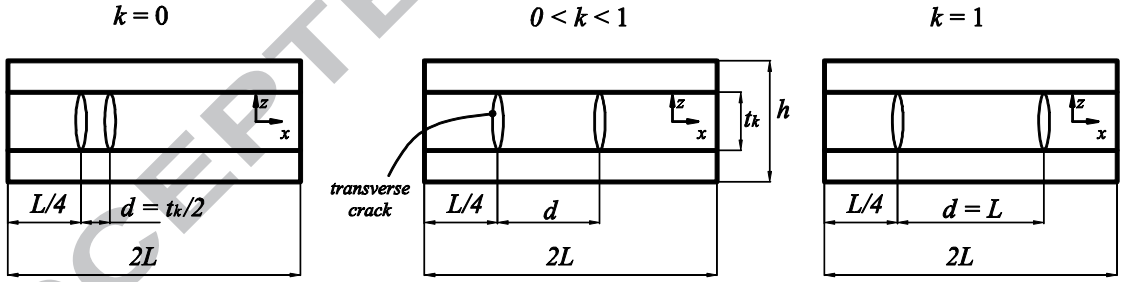

Figure 1: Example of a RVE of a laminate $[0/90]_S$ and the corresponding value of the non-uniformity parameter k.

2.1 Periodic boundary conditions

In this work, Periodic Boundary Conditions (PBC) in the form presented by Piezel *et al.* [32] are used at the RVE boundary. This form of PBC connects the kinematics of a three-

dimensional first order continuum in the meso-scale and the kinematics of a thin flat plate at the macro-scale as follows

$$\vec{u}_r^{+} - \vec{u}_r^{-} = \left(\boldsymbol{\varepsilon}^0 + z\boldsymbol{\kappa}\right)\cdot\left(\vec{x}_r^{+} - \vec{x}_r^{-}\right) \tag{2}$$

$$u_z^{+} - u_z^{-} = -\frac{1}{2}\boldsymbol{\kappa} : \left(\vec{x}_r^{+}\vec{x}_r^{+} - \vec{x}_r^{-}\vec{x}_r^{-}\right) \tag{3}$$

where $\boldsymbol{\varepsilon}^0$ and $\boldsymbol{\kappa}$ are the small strain tensor and curvature tensor in the middle plane of the laminate model, respectively; $\vec{u}_r$ and u_z are the in-plane (directions *x* and *y*) and out-of-plane (direction *z*) projections of the meso-scale displacement of a point at the RVE boundary; *z* is the out-of-plane coordinate, and $\vec{x}_r$ are the coordinates in directions *x* and *y* of points at the RVE boundary. Upper indexes "+" or "-", in equations (2) and (3), refer to pairs of points placed on a pair of faces "Fr - Po", "R - Le" or edges "E2 - E1", "E3 - E1" and "E4 - E1", as shown in Figure 2b.

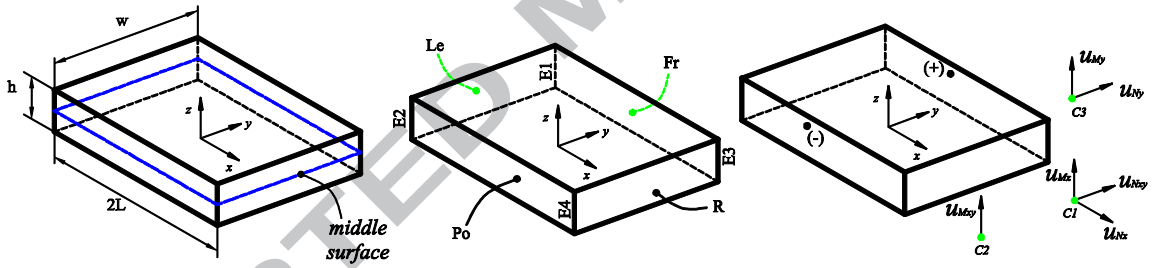

a) b) c)

Figure 2: Representative volume element: a) Dimensions, b) Faces and edges identification and c) Control nodes (C1, C2 and C3) and associated degrees of freedom.

In this work, the PBCs were implemented using the Elimination of Redundant Unknowns (ERU) technique [37]. Six degrees of freedom are added to the Finite Element model and the associated nodes are known as "control nodes", as shown in Figure 2c (points C1, C2 and C3). Notice that the location of control nodes is not relevant. The ERU technique implements equations (2) and (3) by relating the displacements of two points at the RVE boundary with the degrees of freedom of control nodes by means of the following equations

$$u_x^+ - u_x^- - \frac{u_{Nx}}{\alpha_u}\left(x_x^+ - x_x^-\right) - \frac{u_{Nxy}}{\alpha_u}\left(x_y^+ - x_y^-\right) - \frac{u_{Mx}}{\alpha_u^2} z\left(x_x^+ - x_x^-\right) - \frac{u_{Mxy}}{\alpha_u^2} z\left(x_y^+ - x_y^-\right) = 0 \tag{4}$$

$$u_y^+ - u_y^- - \frac{u_{Nxy}}{\alpha_u}\left(x_x^+ - x_x^-\right) - \frac{u_{Ny}}{\alpha_u}\left(x_y^+ - x_y^-\right) - \frac{u_{Mxy}}{\alpha_u^2} z\left(x_x^+ - x_x^-\right) - \frac{u_{My}}{\alpha_u^2} z\left(x_y^+ - x_y^-\right) = 0 \tag{5}$$

$$u_z^+ - u_z^- + \frac{u_{Mx}}{2\alpha_u^2}\left(x_x^{(+)2} - x_x^{(-)2}\right) + \frac{u_{Mxy}}{\alpha_u^2}\left(x_x^+ x_y^+ - x_x^- x_y^-\right) + \frac{u_{My}}{2\alpha_u^2}\left(x_y^{(+)2} - x_y^{(-)2}\right) = 0 \tag{6}$$

and then the following boundary conditions are applied to the degrees of freedom of such control nodes

$$\begin{aligned} &u_{Nx} = \alpha_u \varepsilon_{xx}^0; \quad u_{Ny} = \alpha_u \varepsilon_{yy}^0; \quad u_{Nxy} = \alpha_u \varepsilon_{xy}^0 \\ &u_{Mx} = \alpha_u^2 \kappa_{xx}; \quad u_{My} = \alpha_u^2 \kappa_{yy}; \quad u_{Mxy} = \alpha_u^2 \kappa_{xy} \end{aligned} \tag{7}$$

where ε_{xx}^0, ε_{yy}^0, ε_{xy}^0, κ_{xx}, κ_{yy}, and κ_{xy} are the components of the small strain tensor and curvature in the middle plane of the laminate. Equations (4) - (7) include a unitary factor α_u with units of length to achieve dimensional consistency. Equations (4) - (6) were implemented for faces and edges identified in Figure 2b using the ABAQUS [36] command *EQUATION, which allows the user to implement linear combinations of degrees of freedom in the Finite Element model. In this way, as boundary conditions (7) are imposed at control nodes, the Finite Element model returns a force in each degree of freedom. The displacements and forces at these control nodes are used next to obtain the stress resultants on the macro-scale.

2.2 Evaluation of stress resultants

Considering a thin laminated plate at the macro-scale with middle plane area *S*, and using the Classical Lamination Theory (CLT; [4]), the developed internal power at time *t*, $P_{int}(t)$, is given by [38]

$$P_{int}(t) = S\left(N_x \dot{\varepsilon}_x^0 + N_y \dot{\varepsilon}_y^0 + 2N_{xy}\dot{\varepsilon}_{xy}^0 + M_x \dot{\kappa}_x + M_y \dot{\kappa}_y + 2M_{xy}\dot{\kappa}_{xy}\right) \tag{8}$$

where N_x, N_y and N_{xy} are the forces per unit length and M_x, M_y and M_{xy} are moments per unit length at the middle surface of the laminate. The dot above a variable stands for derivative with respect to time. Such forces and moments are identified as stress resultants in CLT. As stated by the balance of mechanical energy [39], in the meso-scale, containing a three-dimensional Finite Element model with control nodes in a quasi-static problem, the internal power developed by the three-dimensional stress state is equal to the external power P_{ext}. Notice that if the problem is quasi-static, variables can still change with time. This external power P_{ext} at time t is developed by the forces acting at control nodes and can be expressed as

$$P_{ext}(t) = R_{Nx}\dot{u}_{Nx} + R_{Ny}\dot{u}_{Ny} + R_{Nxy}\dot{u}_{Nxy} + R_{Mx}\dot{u}_{Mx} + R_{My}\dot{u}_{My} + R_{Mxy}\dot{u}_{Mxy} \tag{9}$$

where R_{Nx}, R_{Ny}, R_{Nxy}, R_{Mx}, R_{My}, and R_{Mxy} are the forces acting on control nodes and they correspond to the degrees of freedom u_{Nx}, u_{Ny}, u_{Nxy}, u_{Mx}, u_{My}, and u_{Mxy}, respectively, shown in Figure 2c. Then, taking into account the implementation of the PBC, through equations (4) - (7), the external power becomes

$$P_{ext}(t) = \alpha_u \left(R_{Nx}\dot{\varepsilon}_x^0 + R_{Ny}\dot{\varepsilon}_y^0 + R_{Nxy}\dot{\varepsilon}_{xy}^0 \right) + \alpha_u^2 \left(R_{Mx}\dot{\kappa}_x + R_{My}\dot{\kappa}_y + R_{Mxy}\dot{\kappa}_{xy} \right) \tag{10}$$

Following the Hill-Mandel principle, the internal power P_{int} at macro-scale must be equal to the power developed in the meso-scale [40]. Therefore, the next equation holds at time t

$$P_{int}(t) = P_{ext}(t) \tag{11}$$

Then, using equations (8) and (10) into equation (11), and taking derivatives with respect to the deformation rates, $\dot{\varepsilon}_x^0$, $\dot{\varepsilon}_y^0$, and $\dot{\varepsilon}_{xy}^0$; and with respect to the curvature rates $\dot{\kappa}_x$, $\dot{\kappa}_y$, and $\dot{\kappa}_{xy}$, a set of equations arises for the evaluation of stress resultants

$$\begin{aligned} N_x &= \frac{\alpha_u R_{Nx}}{S};\ N_y = \frac{\alpha_u R_{Ny}}{S};\ N_{xy} = \frac{\alpha_u R_{Nxy}}{2S} \\ M_x &= \frac{\alpha_u^2 R_{Mx}}{S};\ M_y = \frac{\alpha_u^2 R_{My}}{S};\ M_{xy} = \frac{\alpha_u^2 R_{Mxy}}{2S} \end{aligned} \tag{12}$$

Equations (12) are based on equivalence of powers in both scales (Hill-Mandel principle) and have the advantage that numerical integration at the RVE is avoided. A similar procedure to obtain the macroscopic stress resultants have been presented by other authors ([3], [32], [20], [34]).

2.3 Evaluation of laminate stiffness matrix

The constitutive equations for the thin laminated plate of the macro-scale are given by [4]

$$\begin{Bmatrix} N_x \\ N_y \\ N_{xy} \\ M_x \\ M_y \\ M_{xy} \end{Bmatrix} = \begin{bmatrix} A_{11} & A_{12} & A_{16} & B_{11} & B_{12} & B_{16} \\ A_{12} & A_{22} & A_{26} & B_{12} & B_{22} & B_{26} \\ A_{16} & A_{26} & A_{66} & B_{16} & B_{26} & B_{66} \\ B'_{11} & B'_{12} & B'_{16} & D_{11} & D_{12} & D_{16} \\ B'_{12} & B'_{22} & B'_{26} & D_{12} & D_{22} & D_{26} \\ B'_{16} & B'_{26} & B'_{66} & D_{16} & D_{26} & D_{66} \end{bmatrix} \begin{Bmatrix} \varepsilon_x^0 \\ \varepsilon_y^0 \\ 2\varepsilon_{xy}^0 \\ \kappa_x \\ \kappa_y \\ 2\kappa_{xy} \end{Bmatrix}; \quad \begin{Bmatrix} N_x \\ N_y \\ N_{xy} \\ M_x \\ M_y \\ M_{xy} \end{Bmatrix} = [S] \begin{Bmatrix} \varepsilon_x^0 \\ \varepsilon_y^0 \\ 2\varepsilon_{xy}^0 \\ \kappa_x \\ \kappa_y \\ 2\kappa_{xy} \end{Bmatrix} \tag{13}$$

The 6×6 laminate stiffness matrix [*S*], in equation (13), is often considered to be composed by 3×3 matrices: *in-plane stiffness* [*A*], *bending-extension coupling* [*B*] and [*B'*], and the *bending stiffness* matrices [*D*]. In order to obtain the coefficients of [*S*], six strain states were applied throughout equations (7). The applied strain states, as is usually done in the homogenization field, have a unique nonzero strain component and, using stress resultants given by (12), the stiffness matrix coefficients are obtained from (13). Notice that for a given strain state the complete corresponding column in matrix [*S*] can be obtained.

3 Results

This section presents a convergence study, then a comparison with numerical and experimental data, followed by a parametric study in cross-ply laminates. The laminate analyzed for the convergence test is conformed by transversely isotropic laminas with Laminate Stacking Sequence (LSS) $[0/90_2/0_{1/2}]_S$ and material properties given by Smith and Ogin [41] as: E_1 = 45.6 GPa, E_2 = 16.2 GPa, G_{12} = 5.83 GPa, ν_{12} = 0.278, ν_{23} = 0.4, with ply thickness t_k = 0.125 mm. The convergence study was performed for the bending stiffness coefficient D_{11} of a

laminate with crack density λ = 4 mm^{-1} in one of the 90 degree laminas. Up to four layers of Finite Elements in the *y* direction were included in the mesh, but just one layer of elements was sufficent. A percent error is defined as

$$Error = \frac{|D_{11} - D_{11Max}|}{D_{11Max}} \times 100 \tag{14}$$

where D_{11} is the obtained coefficient for a given number of elements and D_{11Max} = 1.8806 [GPa mm^3] is the value of the coefficient corresponding to the maximum number of elements used in the analysis, with one layer of Finite Elements in *y* direction. Figure 3 shows the percent error as a function of the number of elements in the Finite Element mesh using quadratic 20-noded brick elements. Acceptable errors can be seen for a small number of elements and convergence is also identified.

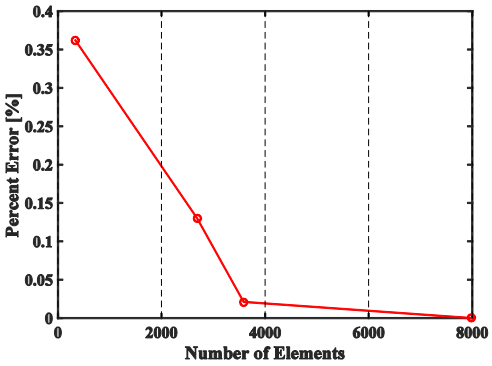

Figure 3: Percentage error as a function of the number of elements for coefficient D_{11} of a laminate with $[0/90_2/0_{1/2}]_S$ and crack density λ = 4 mm^{-1} in the bottom 90 degree lamina.

3.1 Model verification

In order to verify results of the present model, the laminate stiffness matrix [*S*] in equation (13) is obtained and compared with results from the literature for an undamaged and a damaged cross-ply laminate with the laminate data used for the convergence study. In this section, only uniform crack distributions were considered.

The CLT was used to compare results for the laminate without damage; Table 1 shows

the values obtained for the non-zero coefficients in equation (13). The results obtained by the present methodology showed an excellent agreement with CLT results, since all digits shown for the coefficients in Table 1 are the same for both methodologies. Also, for both approaches, the coefficients A_{16}, A_{26}, D_{16}, D_{26}, and all elements of [B] and [B'] matrices resulted in small numbers approaching zero, according with a symmetric cross-ply laminate.

Table 1. Stiffness matrix coefficients using CLT for an intact laminate.

A_{11} [GPa mm]	25.9114	D_{11} [GPa mm^3]	2.0075
A_{22} [GPa mm]	29.6902	D_{22} [GPa mm^3]	1.5400
A_{12} [GPa mm]	4.0519	D_{12} [GPa mm^3]	0.2585
A_{66} [GPa mm]	5.1013	D_{66} [GPa mm^3]	0.3255

Further, to verify the model results for a damaged laminate, the same LSS $[0/90_2/0_{1/2}]_S$ is considered in which one of the 90 degree laminas has a crack density λ and bending curvatures are applied. Figure 4 shows the results for coefficient D_{11} of the laminate as a function of the crack density λ in the cracking 90 degree lamina obtained by the present methodology, CLT, Smith and Ogin [41], and the Ply Discount method. A good agreement can be seen for a wide range of crack densities.

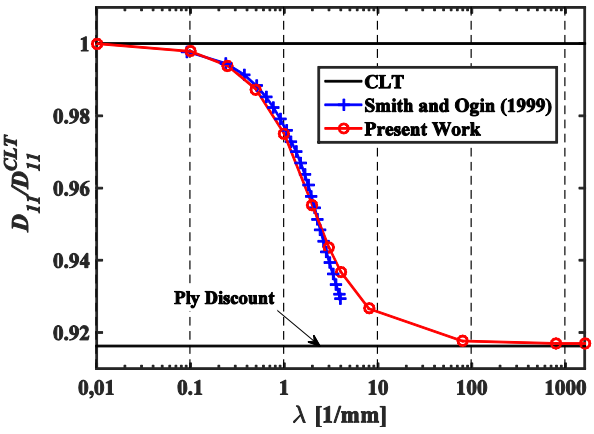

Figure 4: Coefficient D_{11} normalized with respect to Classical Lamination Theory (CLT) results as a function of crack density λ in the 90 degree lamina located on the traction side of the laminate.

3.2 Comparison with experimental results

This section presents a comparison between the model described in Section 2, accounting for uniform and non-uniform crack distributions, and experimental data presented by Varna *et al.*, [42]. The material properties correspond to a glass/epoxy transversely isotropic unidirectional composite with E_1 = 44.7 GPa, E_2 = 12.7 GPa, G_{12} = 5.8 GPa G_{23} = 4.5 GPa, ν_{12} = 0.297 and t_k = 0.144 mm. The laminate has a staking sequence $[0/90_8/0_{1/2}]_S$ and the applied tensile loads generated cracks in both 90 degree laminas with a crack density λ.

Varna *et al.* [42] reported the equivalent in-plane modulus E_x under tensile loads and the equivalent in-plane Poisson ratio ν_{xy}; the relationship among stiffness coefficients and equivalent laminate properties is given by [4]

$$E_x = \frac{A_{11}A_{22} - A_{12}^2}{hA_{22}}; \quad \nu_{xy} = \frac{A_{12}}{A_{22}} \tag{15}$$

where h is the laminate thickness. Figure 5a and 5b show the results for E_x and ν_{xy} obtained from the present model for uniform (k = 1) and non-uniform (k = 0) crack distributions and the experimental results reported by Varna *et al.* [42].

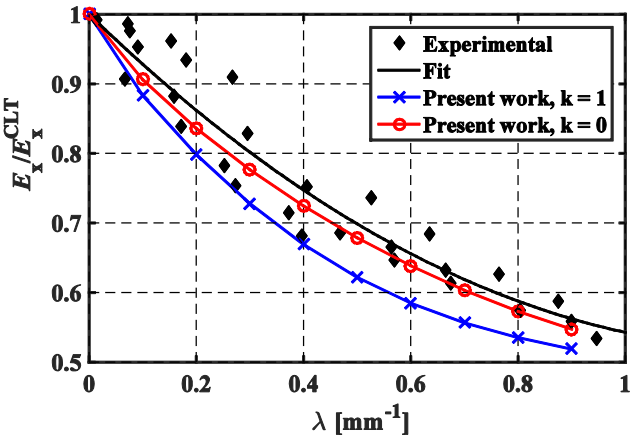

(a)

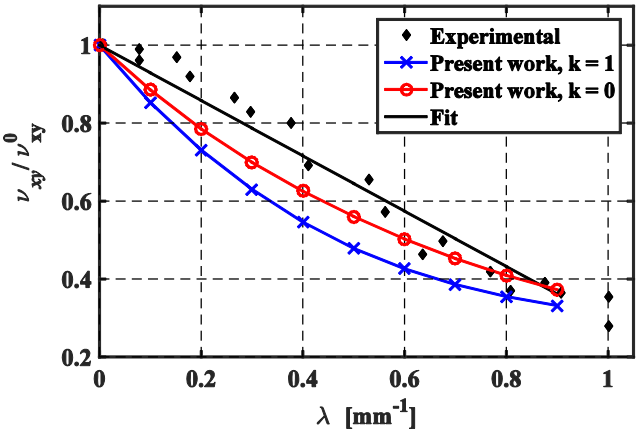

(b)

Figure 5: Comparison of results for uniform (k = 1), non-uniform (k = 0) crack distributions and experimental data from Varna *et al.* [42]: the laminate staking sequence $[0/90_8/0_{1/2}]_S$ with a crack density λ only in the 90 degree laminas. a) Equivalent in-plane modulus E_x and; b) Equivalent in-plane Poisson ratio ν_{xy}.

For reference, a quadratic and a linear function for E_x and ν_{xy} were fitted to experimental data using the Least Square Method. The functions resulted in $f_{Ex} = 1 - 0.7481\times\lambda + 0.2909\times\lambda^2$ and $f_{\nu xy} = 1 - 0.7095\times\lambda$. Figure 6 shows the difference between the values of the fitted equations and those of the model for a uniform ($k = 1$) and a non-uniform ($k = 0$) crack distributions expressed as a percentage of the initial (intact) results. It is clearly seen that the model with non-uniform crack distribution ($k = 0$) has a better agreement with experimental data than the model with uniform crack distribution ($k = 1$) in both properties, suggesting that there is an influence of the actual crack distribution on those properties.

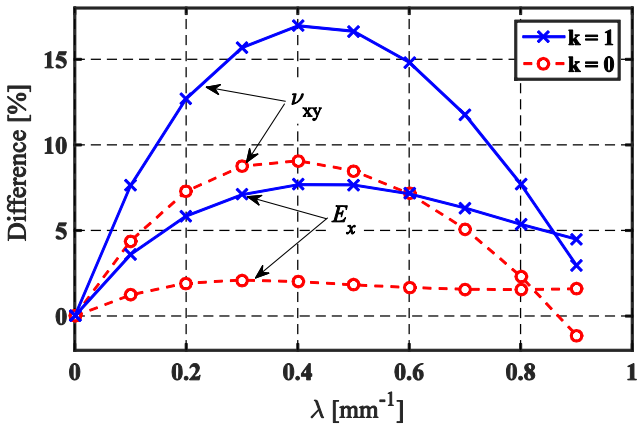

Figure 6: Difference between predictions of the present model (uniform, k = 1; and non-uniform, k = 0) and fitting functions of the experimental data given by Varna *et al.* [42]. Results for the equivalent in-plane Poisson ratio ν_{xy} and equivalent in-plane modulus E_x are expressed as a percentage respect to the initial values. The laminate staking sequence is $[0/90_8/0_{1/2}]_S$ with a crack density λ only in the 90 degree laminas.

Varna *et al.* [42] only presented results for E_x and ν_{xy}, therefore, in the following, the remaining laminated plate properties are analyzed for the same laminate and crack configuration by comparing the predictions for uniform and non-uniform crack distributions.

In-plane shear stiffness A_{66} for the uniform crack distribution was reduced down to 47% percent of the initial (intact) value given by CLT, but the differences between uniform and non-uniform crack distributions were below 1.2%, showing that this stiffness component does not suffer a significant influence due to the crack distribution, despite it suffers a considerable reduction.

The values of D_{11}, D_{12}, D_{22}, and D_{66} for λ = 0.9 mm^{-1} and a uniform crack distribution reached 84.3%, 73.0%, 99.15% and 61.2% of its initial values, respectively. These reductions are not high because the top and bottom layers offer a high stiffness to bending and torsion. The maximum differences between uniform and non-uniform crack distributions reached 2.15%, 3.69%, 0.12%, and 3.4%, respectively.

If the laminate is subjected to curvatures, a coupling is generated among curvatures and in-plane forces, since cracks in one of the 90 degree laminas would be closed. Figure 7a shows the values of 11, 12 and 22 entries of the [*B*] matrix and Figure 7b shows the differences between uniform and non-uniform crack distributions normalized respect to the Ply Discount results; the remaining coefficients of the bending-extension coupling matrix are zero. It can be seen that there is a considerable influence of the crack distribution in those coefficients, reaching a difference of about 12%.

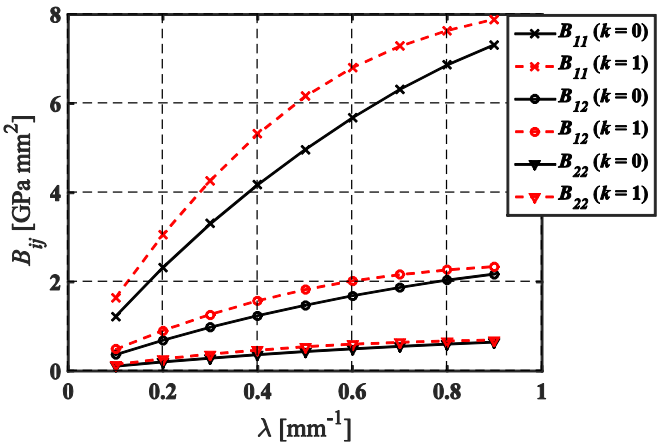

(a)

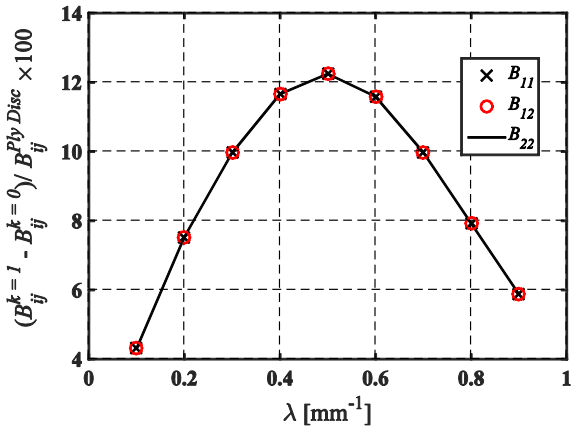

(b)

Figure 7: Results for bending-extension coupling components of a laminate with $[0/90_8/0_{1/2}]_S$ and a crack density λ only in the 90 degree laminas. a) Bending-extension components B_{ij} for uniform (*k*

= 1) and non-uniform (k = 0) crack distributions. b) Difference in results of B_{ij} between uniform and non-uniform crack distributions expressed as a percentage respect to Ply Discount results.

3.3 Parametric study

This section presents a parametric study considering only cross-ply laminates with LSS $[0_n/90_8]_S$ and $[90_8/0_n]_S$, with n = 1 and 8, built in two material systems taken from Barbero *et al.* [19]: glass/epoxy (HyE 9082Af/Fiberite) with transversely isotropic lamina properties E_1 = 44.7 GPa, E_2 = 12.7 GPa, G_{12} = 5.8 GPa G_{23} = 4.5 GPa, ν_{12} = 0.297; and carbon/epoxy (IM6/Avimid K polymer) with E_1 = 134.0 GPa, E_2 = 9.8 GPa, G_{12} = 5.5 GPa G_{23} = 3.6 GPa, ν_{12} = 0.30; the ply thickness is t_k = 0.144 mm. Six laminates were analyzed and, in each laminate, one or two 90 degrees plies were considered having transverse cracks, as shown in Table 2. All laminates were damaged up to saturation defined by a crack density equal to the inverse of the thickness of the cracked ply; the laminates number 1 and 2 were damaged up to λ = 0.434 [mm^{-1}], while the remaining laminates have a maximum crack density λ = 0.868 [mm^{-1}].

Table 2. Laminate staking sequence (LSS) and 90 degree damaged laminas for the analyzed cross-ply laminates.

Laminate number	LSS	90 degree damaged lamina
L1	$[0/90_8]_S$	Middle ply
L2	$[0_8/90_8]_S$	Middle ply
L3	$[90_8/0]_S$	Bottom ply
L4	$[90_8/0_8]_S$	Bottom ply
L5	$[90_8/0]_S$	Bottom and top plies
L6	$[90_8/0_8]_S$	Bottom and top plies

From the results of the above presented model and according to any symmetric cross-ply laminate, the initial (intact) [B] and [B'] bending-extension coupling matrices are zero as well as coefficients A_{16}, A_{26}, D_{16} and D_{26}.

For all damaged laminates, material systems (glass/epoxy and carbon/epoxy) and, for uniform and non-uniform crack distributions, the entries 16 and 26 in matrices [A], [B], [B'],

and [*D*], resulted equal to zero. This characteristic is expected since all analyzed laminates are cross-ply. In addition, the obtained sub-matrices [*A*], [*B*], [*B'*] and [*D*] were all symmetric. Also for all laminates, constants A_{22} and D_{22} did not suffer considerable reductions, since the cracked 90 degree laminas provided the stiffness in these load directions, therefore, no significant differences exist between results for uniform and non-uniform crack distributions in these constants.

Figure 8 shows the values for the non-zero entries of [*A*] matrix in laminates *L1* and *L2*, with LSS $[0/90_8]_S$ and $[0_8/90_8]_S$ (carbon/epoxy) for uniform (k = 1) and non-uniform (k = 0) crack distributions. It can be seen that *L1* has higher reductions in its coefficients than those of *L2*. Some differences can be seen between results for uniform and non-uniform crack distributions. The variables Δ_{Aij}, defined as

$$\Delta_{Aij} = \frac{A_{ij}^{\,k=0} - A_{ij}^{\,k=1}}{A_{ij}^{\,CLT}} \times 100 \tag{16}$$

are the differences between coefficients of uniform and non-uniform crack distributions expressed as a percentage of CLT results.

In Figure 9, Δ_{Aij} are plotted as a function of the crack density for the same laminates *L1* and *L2* as in Figure 8. It can be seen that, as the crack density grows from zero, the predictions of the uniform (k = 1) and non-uniform (k = 0) crack distribution models gradually separate from each other finding a maximum in the differences Δ_{Aij} and then, they tend to approach each other again as the crack density reaches saturation. Figure 9 shows that the higher differences are in A_{12} exceeding 12% and 7% for laminates *L1* and *L2*, respectively. A_{11} show a smaller maximum difference of about 5% in *L1*, whereas the other constants have a difference lower than 5%. An important comment can be done on constant A_{66}: it suffers considerable reductions but is not significantly modified by a non-uniform crack distribution, presenting a maximum difference smaller than 2.5%.

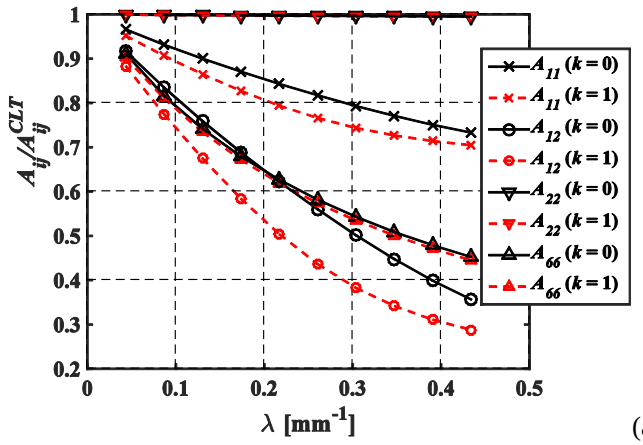

(a)

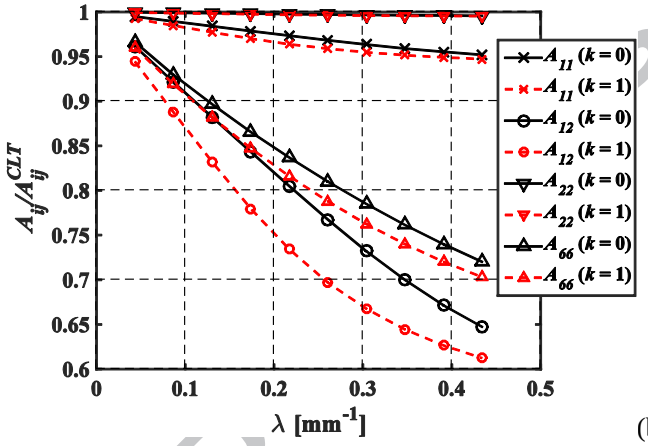

(b)

Figure 8: Values for coefficients A_{ij} normalized respect to CLT results for a carbon/epoxy material system for uniform (k = 1) and non-uniform (k = 0) crack distributions. The middle 90 degree lamina has a crack density λ. (a) $[0/90_8]_S$ laminate *L1*, (b) $[0_8/90_8]_S$ laminate *L2*.

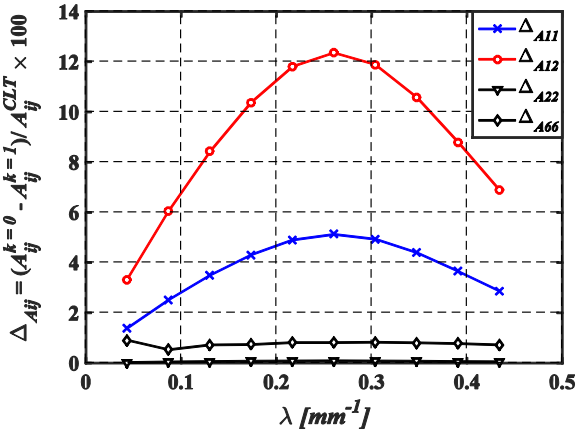

(a)

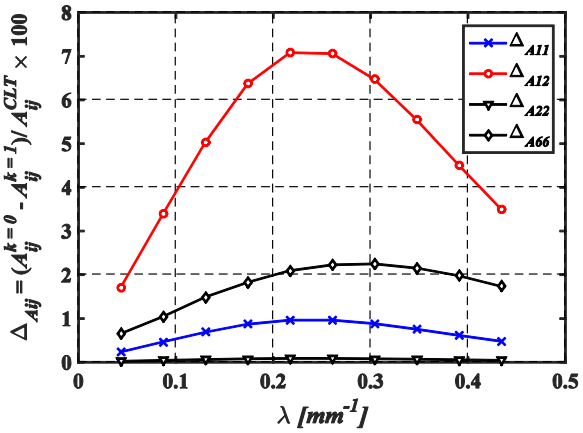

(b)

Figure 9: Difference in results of A_{ij} between uniform (k = 1) and non-uniform (k = 0) crack distributions expressed as a percentage respect to CLT results for a carbon/epoxy material system. (a) $[0/90_8]_S$ laminate *L1*, (b) $[0_8/90_8]_S$ laminate *L2*. The middle 90 degree lamina has a crack density λ.

Table 3 reports the values of stiffness coefficients A_{ij}, D_{ij} and B_{ij} for uniform crack distribution (k = 1), corresponding to the saturation crack density from laminates *L1* to *L6* and both carbon/epoxy and glass/epoxy material systems. The results of A_{ij} and D_{ij} are normalized with respect to CLT values, while the B_{ij} are normalized with respect to Ply Discount values. The maximum values of Δ_{Aij} found in each laminate are reported in Table 4, together with the differences Δ_{Dij} and Δ_{Bij} defined as

$$\Delta_{Dij} = \frac{D_{ij}^{\,k=0} - D_{ij}^{\,k=1}}{D_{ij}^{\,CLT}} \times 100; \quad \Delta_{Bij} = \frac{B_{ij}^{\,k=1} - B_{ij}^{\,k=0}}{B_{ij}^{\,Ply\ \ Discount}} \times 100 \tag{17}$$

Notice that these maximum values of Δ_{Aij}, Δ_{Dij} and Δ_{Bij} do not correspond to saturation but smaller crack densities, as can be seen in Figure 9 for Δ_{Aij}.

Among all cases for in-plane stiffness matrix [*A*], it is seen that A_{12} presented the highest differences due to non-uniformly distributed cracks exceeding 5% in all cases except in *L4*, and reaching about 15% in *L5* built in carbon/epoxy. Constant A_{11} was less affected by a non-uniform crack distribution showing Δ_{A11} greater than 5% only for laminates *L1* and *L5* in

both material systems. Finally, constant A_{66} was reduced down to 30% in *L5* and 80% in *L4* but, regardless of the high or low reduction, the differences in A_{66} between uniform and non-uniform crack distributions were smaller than 5% in all cases. This shows A_{66} as a constant that could be highly reduced by transverse cracks but such reduction does not depend on the actual crack distribution.

Table 3. Coefficients of matrices [*A*], [*B*] and [*D*] for the saturation crack density in laminates *L1* - *L6* with a uniform crack distribution (k = 1). The results of [*A*] and [*D*] are normalized with respect to CLT values, while the results for [*B*] are normalized respect to Ply Discount values.

	carbon/epoxy						glass/epoxy					
	L1	*L2*	*L3*	*L4*	*L5*	*L6*	*L1*	*L2*	*L3*	*L4*	*L5*	*L6*
A_{11}	0.704	0.947	0.835	0.970	0.673	0.939	0.430	0.824	0.687	0.900	0.380	0.801
A_{12}	0.288	0.612	0.604	0.777	0.212	0.554	0.271	0.603	0.600	0.775	0.207	0.550
A_{22}	0.995	0.995	0.997	0.997	0.994	0.995	0.980	0.985	0.989	0.991	0.978	0.982
A_{66}	0.445	0.703	0.651	0.804	0.297	0.608	0.447	0.705	0.653	0.805	0.299	0.609
B_{11}	0.603	0.588	0.968	0.923	0.967	0.922	0.630	0.612	0.972	0.930	0.970	0.927
B_{12}	0.603	0.588	0.968	0.923	0.967	0.922	0.630	0.612	0.972	0.930	0.970	0.927
B_{22}	0.603	0.588	0.968	0.923	0.967	0.922	0.630	0.612	0.972	0.930	0.970	0.927
B_{66}	-	-	0.863	0.817	-	-	-	-	0.861	0.815	-	-
D_{11}	0.964	0.998	0.515	0.840	0.515	0.840	0.897	0.990	0.508	0.683	0.507	0.683
D_{12}	0.830	0.970	0.507	0.586	0.507	0.585	0.819	0.969	0.506	0.584	0.505	0.583
D_{22}	0.998	0.999	0.997	0.997	0.997	0.997	0.994	0.998	0.988	0.989	0.988	0.989
D_{66}	0.787	0.964	0.574	0.635	0.151	0.269	0.788	0.964	0.575	0.636	0.152	0.271

Table 4. Higher values of the differences in constants between uniform (k = 1) and non-uniform (k = 0) crack distributions (Δ_{Aij}, Δ_{Bij}, and Δ_{Dij}). The differences Δ_{Aij} and Δ_{Dij} are expressed as a percentage of CLT results, and Δ_{Bij} are expressed as a percentage of Ply Discount values. The values greater than 5% are expressed in bold type.

	carbon/epoxy						glass/epoxy					
	L1	*L2*	*L3*	*L4*	*L5*	*L6*	*L1*	*L2*	*L3*	*L4*	*L5*	*L6*
Δ_{A11}	**5.129**	0.965	2.653	0.644	**6.491**	1.403	**6.429**	3.128	3.999	1.929	**9.299**	4.384
Δ_{A12}	**12.36**	**7.080**	**6.389**	4.724	**15.63**	**10.30**	**8.228**	**7.069**	**5.119**	4.359	**11.90**	**9.908**

Δ_{A22}	0.091	0.087	0.047	0.058	0.115	0.126	0.224	0.276	0.139	0.170	0.324	0.387
Δ_{A66}	0.907	2.251	4.427	2.447	3.287	4.676	0.901	2.224	4.417	2.486	3.268	4.701
Δ_{B11}	**6.907**	**7.183**	**17.49**	**20.56**	**16.97**	**20.56**	4.733	**7.270**	**14.09**	**18.99**	**13.37**	**18.97**
Δ_{B12}	**6.905**	**7.179**	**17.49**	**20.56**	**16.97**	**20.56**	4.732	**7.271**	**14.09**	**18.99**	**13.38**	**18.97**
Δ_{B22}	**6.905**	**7.179**	**17.49**	**20.56**	**16.97**	**20.56**	4.732	**7.271**	**14.09**	**18.99**	**13.38**	**18.97**
Δ_{B66}	0.000	0.000	**11.76**	**10.55**	0.000	0.000	0.000	0.000	**11.75**	**10.72**	0.000	0.000
Δ_{D11}	0.308	0.023	**8.920**	3.686	**8.665**	3.684	0.568	0.090	**7.408**	**6.678**	**7.063**	**6.671**
Δ_{D12}	1.472	0.278	**9.075**	**9.525**	**8.816**	**9.521**	0.993	0.287	**7.434**	**8.782**	**7.087**	**8.773**
Δ_{D22}	0.013	0.010	0.060	0.071	0.058	0.071	0.032	0.019	0.186	0.242	0.178	0.241
Δ_{D66}	1.175	0.173	**5.858**	4.824	**15.11**	**10.03**	1.165	0.166	**5.863**	4.898	**15.17**	**10.27**

Figure 10 shows the values of constants D_{ij} for laminates *L5* and *L6*, with LSS $[90_8/0]_S$ $[90_8/0_8]_S$, and glass/epoxy material system. There are appreciable reductions in coefficients D_{11} and D_{12} and high reductions in D_{66}. Laminate *L6* presents smaller reductions than *L5* because of the thicker 0 (zero) degree lamina provides a higher stiffness in *L6*. Values of Δ_{Dij} are shown in Figure 11 and, as found for A_{ij}, the differences Δ_{Dij} depend on the crack density presenting a local maximum before reaching saturation. For *L5* and *L6*, the maximum values of the differences Δ_{Dij} exceeded 5%, with exception of Δ_{D22}, reaching about 15% and 10% in Δ_{D66}.

Table 3 shows that the highest reductions in [*D*] happened in D_{66} for laminates *L5* and *L6*. Laminates *L1* and *L2* did not suffer high reductions in the bending stiffness matrix [*D*] because of the undamaged 0 (zero) degree laminas located at the top and at the bottom. On the other hand, laminates *L3* - *L6*, which have external cracks, suffered a notable influence of crack distribution, as shown in Table 4. The difference Δ_{D11} presented values greater than 5% in laminates *L3* - *L6* except for *L4* and *L6* with a carbon/epoxy system. Finally, D_{66} was significantly influenced by the crack distribution when the laminate has external cracks, as in *L5* and *L6*.

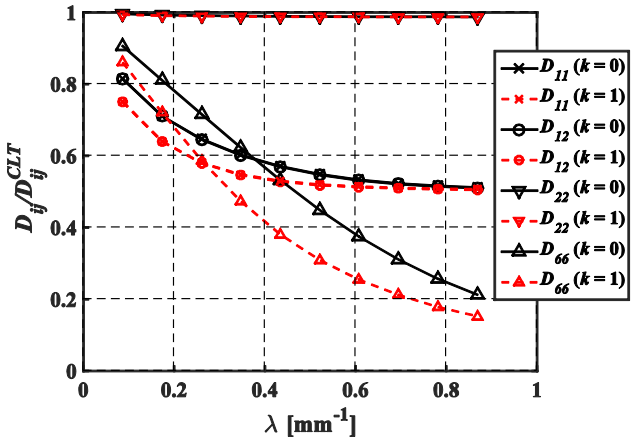

(a)

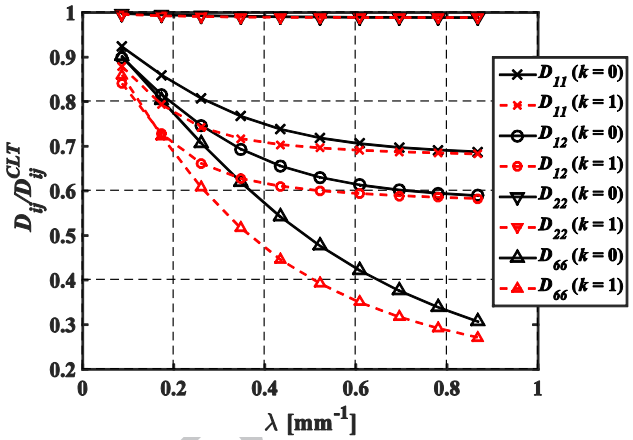

(b)

Figure 10: Values for coefficients D_{ij} normalized respect to CLT results for a glass/epoxy material system for uniform (k = 1) and non-uniform (k = 0) crack distributions. (a) $[90_8/0]_S$ laminate *L5*, (b) $[90_8/0_8]_S$ laminate *L6*. The top and bottom laminas have a crack density λ.

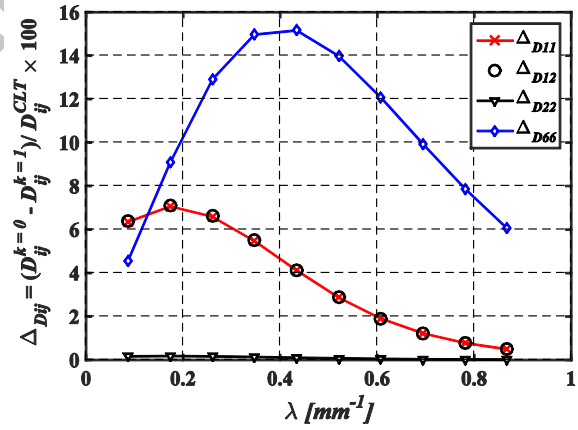

(a)

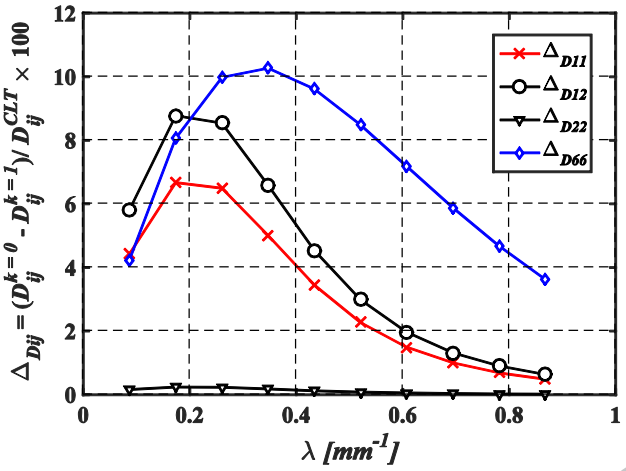

(b)

Figure 11: Difference in results of D_{ij} between uniform (k = 1) and non-uniform (k = 0) crack distributions normalized respect to CLT results for a glass/epoxy material system. (a) $[90_8/0]_S$ laminate *L5*, (b) $[90_8/0_8]_S$ laminate *L6*. The top and bottom 90 degree laminas have a crack density λ.

Laminates 3 and 4, when damaged, presented *bending-extension* coupling; specifically entries 11, 12, 22 and 66 from [*B'*] and [*B*] matrices were non-zero and this is because these laminates are non-symmetrically damaged. Obtained values of [*B*] and [*B'*] are equal. In Figure 12, the [*B*] components are plotted with values normalized respect to the Ply Discount results for *L3* and *L4* with a glass/epoxy material system. The trends in normalized values of B_{ij} are the same for entries 11, 12, and 22. The differences Δ_{Bij} are plotted in Figure 13 in which it can be seen that the differences also depend on the crack densities and, as for Δ_{Aij} and Δ_{Dij}, differences Δ_{Bij} present a local maximum. This Figure shows that all differences Δ_{Bij} exceeded 5% in a wide range on crack densities in *L3* and *L4* (Figure 13).

Table 4 shows that all [*B*] entries reported were significantly influenced by non-uniformly distributed cracks, with exception in *L1* glass/epoxy laminate which showed a difference less than 5%.

Laminates 1, 2, 5, and 6 are symmetrically damaged and consequently, when subjected to membrane deformations or torsion curvatures, the *bending-extension* coupling matrix [*B'*]

had only zero elements and also B_{66} was null. However, when those laminates are subjected to bending curvatures, κ_x or κ_y, at least some part of the crack or, the entire crack, will close and therefore the laminates behave like non-symmetrically damaged ones presenting non-zero values of entries 11, 12, and 22 of the [*B*] matrix, making [*B*] different to [*B'*]. This is showing that the laminate stiffness depends on the interaction between the crack surfaces (crack closure) dictated by the acting strain state.

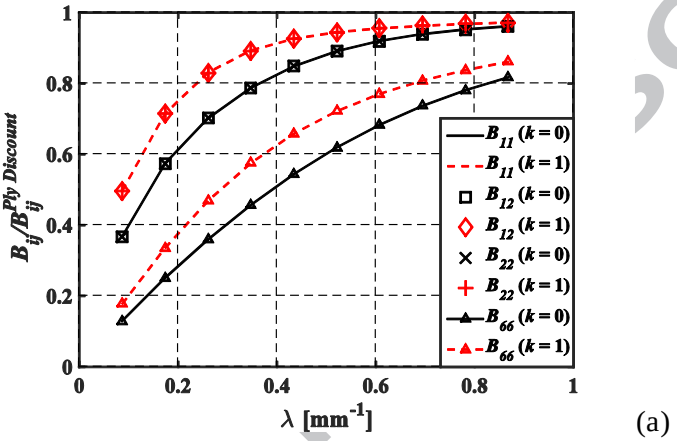

(a)

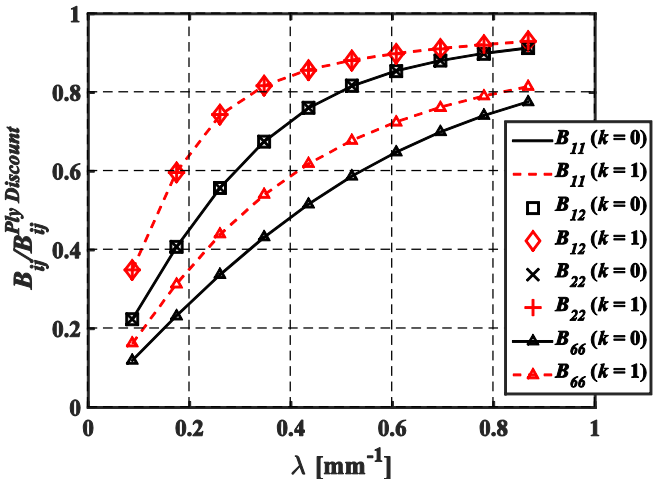

(b)

Figure 12: Values for coefficients B_{ij} normalized respect to Ply Discount results for a glass/epoxy material system for uniform (k = 1) and non-uniform (k = 0) crack distributions. (a) $[90_8/0]_S$ laminate *L3*, (b) $[90_8/0_8]_S$ laminate *L4*. The bottom 90 degree lamina has a crack density λ.

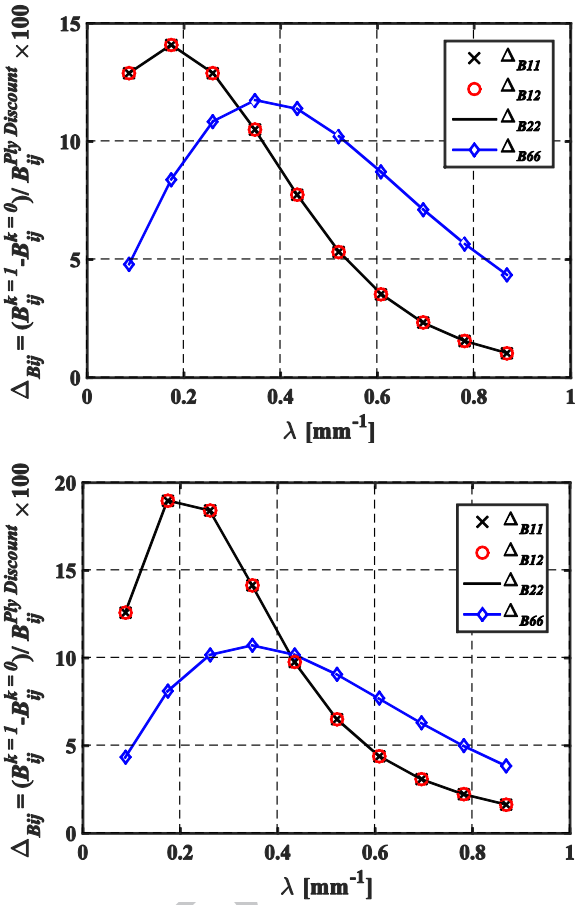

Figure 13: Difference in results of B_{ij} between uniform (k = 1) and non-uniform (k = 0) crack distributions expressed as a percentage respect to Ply Discount results for a glass/epoxy material system. (a) $[90_8/0]_S$ laminate *L3*, (b) $[90_8/0_8]_S$ laminate *L4*. The bottom 90 degree lamina has a crack density λ.

In Figures 14 to 17, some values of [*A*], [*D*], and [*B*] are plotted as a function of the non-uniformity parameter k for selected laminates. As the parameter k approaches unity, the constants approaches the values for uniformly distributed cracks with the derivative of components S_{ij} respect to k approaching zero but without changing sign. Therefore, the higher changes in each constant S_{ij} are located near k = 0.

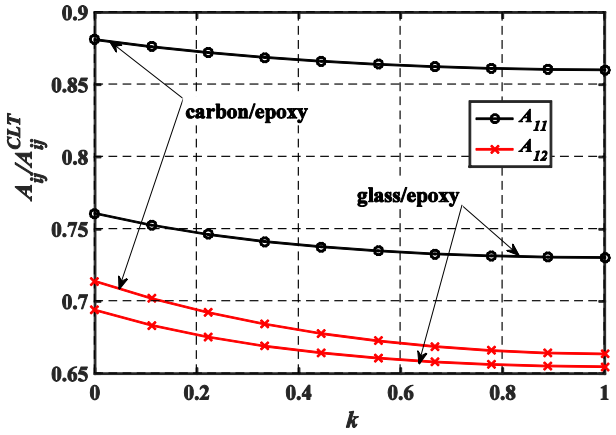

Figure 14: Influence of non-uniformity coefficient k on A_{11} and A_{12} for laminate *L3* $[90_8/0]_S$ with a crack density $\lambda = 0.347$ mm^{-1}; results normalized respect to CLT values.

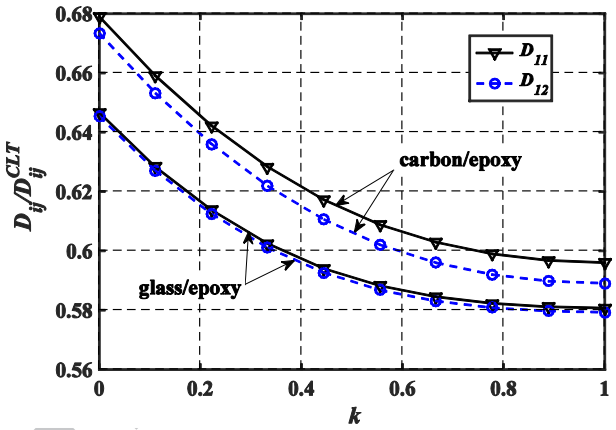

Figure 15: Influence of non-uniformity coefficient k on coefficients D_{11} and D_{12} for laminate *L5* $[90_8/0]_S$ with a crack density $\lambda = 0.26$ mm^{-1}; results normalized respect to CLT values.

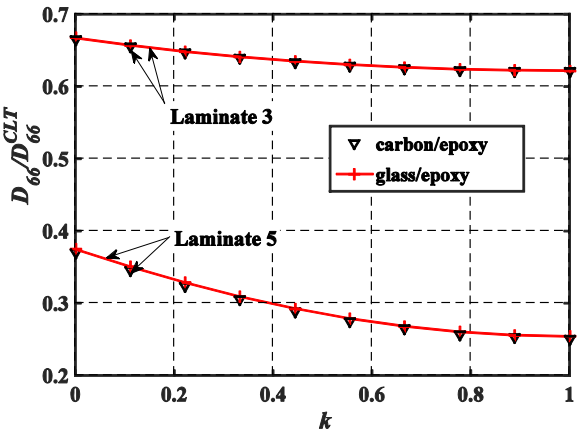

Figure 16: Influence of non-uniformity coefficient k on coefficient D_{66} for laminate *L3* and *L5* $[90_8/0]_S$ with a crack density $\lambda = 0.608$ mm^{-1}; results normalized respect to CLT values.

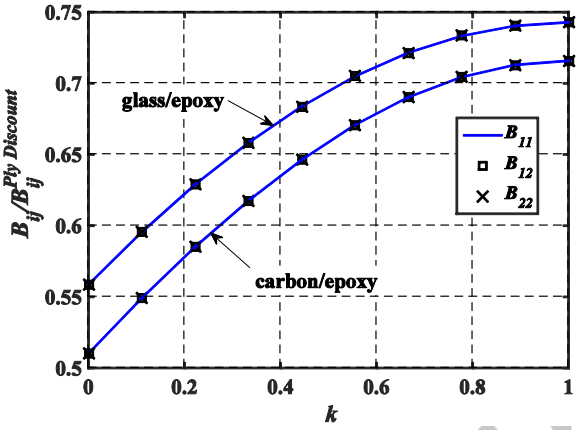

Figure 17: Influence of non-uniformity coefficient k on coefficients B_{11}, B_{12}, and B_{22} for laminate *L4* $[90_8/0_8]_S$ with a crack density $\lambda = 0.26$ mm^{-1}; results normalized respect to Ply Discount values.

In Figure 8 for A_{ij}, and in Figure 10 for D_{ij}, the values given by a model with uniformly distributed cracks (k = 1) are always below the values for the non-uniform crack distribution model (k = 0). Also, in Figures 14, 15, and 16, with an increment in parameter k, the values of A_{ij} and D_{ij} always decrease. In contraposition, Figures 7a and 12, for the B_{ij} constants, show that the uniformly distributed crack model (k = 1) always give higher predictions than those of the model with non-uniform crack distribution (k = 0). Moreover, Figure 17 shows increasing values of B_{ij} with increasing values of k. These results are suggesting that for the elements of matrices [A] and [D] the uniform crack distribution model gives an underestimation; this was pointed out by Loukil *et al.* [29] for the equivalent in-plane laminate modulus E_x. On the other hand, the uniform crack distribution model gives overestimations for the *bending-extension* coupling matrices [B] and [B'].

5 Conclusions

In this work, a computational meso-mechanic model was applied for the evaluation of plate stiffness in cross-ply fiber-reinforced composite laminates of the type $[0_n/90_8]_S$ and $[90_8/0_n]_S$, with n = 1 and 8, including non-uniformly distributed transverse matrix cracks. The meso-scale includes a three-dimensional domain with an elastic Finite Element first order continuum model, called Representative Volume Element (RVE) and spanning the complete laminate thickness, while the domain at the macro-scale corresponds to a classical thin laminated plate. This study considers two fiber reinforced composites: glass/epoxy and carbon/epoxy. Periodic boundary conditions were used in the domain of the meso-scale, allowing the RVE to undergo membrane and bending infinitesimal deformations. For the implementation of boundary conditions, the technique of Elimination of Redundant Unknowns was applied using control nodes. Then, the forces on these control nodes were used for the evaluation of the stress resultants with equations obtained from the equivalence of mechanical power in the meso-scale and the macro-scale (Hill-Mandel principle).

The results obtained with the present model showed good agreement with both numerical and experimental data from the literature. Also, the model with a non-uniform crack distribution presented better agreement with experimental data than the model with uniformly distributed cracks, suggesting the existence of an influence of the non-uniformity of crack distribution on laminate stiffness.

In a parametric study, it is shown that the in-plane stiffness coefficients presents differences between uniform and non-uniform configurations that can reach about 12% of the initial undamaged results. However, the in-plane shear stiffness is not influenced by the crack distribution although it can be highly reduced by transverse matrix cracks. The bending stiffness is significantly influenced only in laminates with external cracks and, specifically, the torsional stiffness suffers a notable influence by the non-uniform crack distribution in those laminates. The highest influence of non-uniformly distributed cracks was found on the bending-extension coupling matrix which showed differences between uniform and non-uniformly

located cracks of about 20% respect to the values of Ply Discount approach.

The results suggest that, for initially symmetric cross-ply laminates, the predictions for the elements of the in-plane and bending stiffness matrices given by the model with uniformly distributed cracks are always underestimations, whereas the same model with uniform crack distribution overestimates the values of the bending-extension coupling matrices.

Acknowledgments

NDB and LAG were supported by CONICET, the Science Research Council of Argentina during this research. The authors thank the support received from grants of CONICET (PIP 0126), SECyT-UNC, and UTN-FRC (UTI 2119).

References

[1] Barbero EJ, Cabrera Barbero J. Analytical solution for bending of laminated composites with matrix cracks. Compos Struct. 2016 ;135:140-55.

[2] Adolfsson E, Gudmundson P. Matrix crack induced stiffness reductions in $[(0_m/90_n/+\theta_p/-\theta_q)_S]_M$ composite laminates. Compos Eng. 1995;5(1):107-23.

[3] Adolfsson E, Gudmundson P. Thermoelastic properties in combined bending and extension of thin composite laminates with transverse matrix cracks. Int J Solids Struct. 1997;34(16):2035-2060.

[4] Barbero EJ. Introduction to Composite Materials Design. CRC press. Boca Ratón; 2010.

[5] Pupurs A, Varna J, Loukil M, Kahla HB, Mattsson D. Effective stiffness concept in bending modeling of laminates with damage in surface 90-layers. Compos A Appl Sci Manuf. 2016;82:244-252.

[6] Barbero EJ, Cortes DH. A mechanistic model for transverse damage initiation, evolution, and stiffness reduction in laminated composites. Compos B Eng. 2010;41(2):124-132.

[7] Carraro PA, Quaresimin M. A stiffness degradation model for cracked multidirectional laminates with cracks in multiple layers. Int J Solids Struct. 2015;58:34-51.

[8] Hashin Z. Analysis of cracked laminates: A variational approach. Mech Mater. 1985;4(2):121-136.

[9] Hajikazemi M, Sadr MH, Talreja R. Variational analysis of cracked general cross-ply laminates under bending and biaxial extension. Int J Damage Mech. 2015;24(4):582-624.

[10] Hajikazemi M, Sadr MH, Varna J. Analysis of cracked general cross-ply laminates under general bending loads: A variational approach. J Compos Mater. 2017; 51(22): 3089-3109.

[11] Makins RK, Adali S. Bending of cross-ply laminated plates with matrix cracks. The Journal of Strain Analysis for Engineering Design. 1991;26(4):253-7.

[12] Dvorak GJ, Laws N, Hejazi M. Analysis of progressive matrix cracking in composite laminates I. Thermoelastic properties of a ply with cracks. J Compos Mater. 1985;19(3):216-34.

[13] Fan Y, Wang H. Nonlinear bending and postbuckling analysis of matrix cracked hybrid laminated plates containing carbon nanotube reinforced composite layers in thermal environments. Compos Part B-Eng. 2016;86:1-6.

[14] Lei ZX, Yin BB, Liew KM. Bending and vibration behaviors of matrix cracked hybrid laminated plates containing CNTR-FG layers and FRC layers. Compos Struct. 2018;184:314-326.

[15] Lei ZX, Zhang LW, Liew KM. Modeling large amplitude vibration of matrix cracked hybrid laminated plates containing CNTR-FG layers. Appl Math Model. 2017. https://doi.org/10.1016/j.apm.2017.10.032

[16] Adumitroaie A, Barbero EJ. Intralaminar damage model for laminates subjected to membrane and flexural deformations. Mech Adv Mater Struct. 2015;22(9):705-716.

[17] Montesano J, Singh CV. A synergistic damage mechanics based multiscale model for composite laminates subjected to multiaxial strains. Mech Mater. 2015;83:72-89.

[18] Li S, Singh CV, Talreja R. A representative volume element based on translational symmetries for FE analysis of cracked laminates with two arrays of cracks. Int J Solids Struct. 2009;46(7):1793-1804.

[19] Barbero EJ, Cosso FA, Campo FA. Benchmark solution for degradation of elastic properties due to transverse matrix cracking in laminated composites. Compos Struct. 2013;98:242-252.

[20] Schmitz A, Horst P. A finite element unit-cell method for homogenised mechanical properties of heterogeneous plates. Compos A App Sci Manuf. 2014;61:23-32.

[21] Ghayour M, Hosseini-Toudeshky H, Jalalvand M, Barbero EJ. Micro/macro approach for prediction of matrix cracking evolution in laminated composites. J Compos Mater. 2016;50(19):2647-2659.

[22] Adumitroaie A, Barbero EJ, Schagerl M. Matrix cracking in non-symmetric laminates under combined membrane and flexural loading. Int J Mater Mech Man. 2016;4:223-31.

[23] Li S, Reid SR, Soden PD. A finite strip analysis of cracked laminates. Mech Mater. 1994;18(4):289-311.

[24] Hu H, Li S, Wang J, Wang Y, Zu L. FBG-based real-time evaluation of transverse cracking in cross-ply laminates. Compos Struct. 2016;138:151-160.

[25] Silberschmidt VV. Matrix cracking in cross-ply laminates: effect of randomness. Compos A App Sci Manuf. 2005;36(2):129-135.

[26] Wang AS, Chou PC, Lei SC. A stochastic model for the growth of matrix cracks in composite laminates. J Compos Mater. 1984;18(3):239-254.

[27] Silberschmidt VV. Effect of micro-randomness on macroscopic properties and fracture of laminates. J Mater Sci. 2006;41(20):6768-6776.

[28] McCartney LN, Schoeppner GA. Predicting the effect of non-uniform ply cracking on the thermoelastic properties of cross-ply laminates. Compos Sci Technol. 2002;62(14):1841-1856.

[29] Loukil MS, Varna J, Ayadi Z. Applicability of solutions for periodic intralaminar crack distributions to non-uniformly damaged laminates. J Compos Mater. 2013;47(3):287-301.

[30] Noh J, Whitcomb J. Effect of various parameters on the effective properties of a cracked ply. J Compos Mater. 2001;35(8):689-712.

[31] Lundmark P, Varna J. Crack face sliding effect on stiffness of laminates with ply cracks.

Compos Sci Technol. 2006;66(10):1444-1454.

[32] Piezel B, Mercatoris BC, Trabelsi W, Laiarinandrasana L, Thionnet A, Massart TJ. Bending effect on the risk for delamination at the reinforcement/matrix interface of 3D woven fabric composite using a shell-like RVE. Compos Struct. 2012;94(8):2343-2357.

[33] Fillep S, Mergheim J, Steinmann P. Towards an efficient two-scale approach to model technical textiles. Comput Mech. 2017;59(3):385-401.

[34] Yoshida K, Nakagami M. Numerical analysis of bending and transverse shear properties of plain-weave fabric composite laminates considering intralaminar inhomogeneity. Adv Compos Mater. 2017;26(2):135-156.

[35] Petracca M, Pelà L, Rossi R, Oller S, Camata G, Spacone E. Multiscale computational first order homogenization of thick shells for the analysis of out-of-plane loaded masonry walls. Comput Method Appl M. 2017;315:273-301.

[36] Abaqus v. 6.7, 2009. Dassault Systèmes, Providence, RI, USA.

[37] Otero F, Oller S, Martinez X, Salomón O. Numerical homogenization for composite materials analysis. Comparison with other micro mechanical formulations. Compos Struct. 2015;122:405-416.

[38] Cecchi A, Milani G, Tralli A. A Reissner–Mindlin limit analysis model for out-of-plane loaded running bond masonry walls. Int J Solids Struct. 2007;44(5):1438-1460.

[39] Holzapfel GA. Nonlinear Solid Mechanics. Chichester. Wiley; 2000.

[40] de Souza Neto EA, Feijóo RA. On the equivalence between spatial and material volume averaging of stress in large strain multi-scale solid constitutive models. Mech Mater. 2008;40(10):803-811.

[41] Smith PA, Ogin SL. On transverse matrix cracking in cross-ply laminates loaded in simple bending. Compos A App Sci Manuf. 1999;30(8):1003-1008.

[42] Varna J, Joffe R, Akshantala NV, Talreja R. Damage in composite laminates with off-axis plies. Compos Sci Technol. 1999;59(14):2139-2147.